Beam driven electron acceleration to 4 GeV at Gemini

Contact: michael.backhouse13@imperial.ac.uk

M. P. Backhouse, R. Luo, J. Hills, L. Kennedy, C. Cobo, E. Los, Z. Najmudin
The John Adams Institute
Imperial College London
SW7 2BZ, United Kingdom

N. Lopes
GoLP/Instituto de Plasmas e Fusão Nuclear
Instituto Superior Técnico
1049-001 Lisboa, Portugal

E. Gerstmayr, J. Sarma, G. Sarri
School of Mathematics and Physics
Queen's University Belfast
BT7 1NN, United Kingdom

P. Blum, R. J. Shalloo
Deutsches Elektronen-Synchrotron DESY,
Notkestr. 85, 22607 Hamburg, Germany

N. Bourgeois
Central Laser Facility
Rutherford Appleton Laboratory, Didcot
OX11 0QX, United Kingdom

Abstract

We present measurements of electrons accelerated to high energies using both beams of the Gemini laser system. Two independent gas cells were used, placed within 10 mm of each other, with a thin-film plasma mirror placed between them to couple the laser pulses compactly. Electron beams with peak energies of approximately 1 GeV were generated in the first cell via laser wakefield acceleration. The beams were then further spectrally modified by the presence of plasma in the second cell. This resulted in the acceleration of parts of the beam up to the measurement threshold of the spectrometer, with energies reaching $(4.0^{+0.4}_{-0.3})$ GeV. This further acceleration is consistent with beam-driven acceleration of the trailing part of the electron beam. These results could have implications for future implementations of the laser-plasma wakefield accelerator concept.

1 Introduction

The extreme electric fields that plasmas can support may be used to accelerate electrons to high energies over short distances. A fast-travelling driver can excite a rapidly moving plasma wave, and electrons trapped in this wave can extract energy efficiently. In laser wakefield acceleration (LWFA), the driver is the intensity gradient of an ultra-short tightly focused laser pulse, while plasma wakefield acceleration (PWFA) uses the Coulomb force of a relativistic electron bunch to drive the wave. An advantage of LWFA is that it does not require a conventional accelerator to generate the initial driver; instead, it relies on laser pulses that can be produced more compactly and at a lower cost. A disadvantage of LWFA is dephasing, an acceleration limit resulting from the electron beam overtaking the plasma wave. PWFA does not suffer from this since the driver is ultrarelativistic, preserving the phase between the driving and witness bunches. Consequently, a PWFA driven by an LWFA-generated beam theoretically mitigates some of the disadvantages of each scheme [1].

The combined LWFA-PWFA scheme has been used recently to enhance the stability and spectral properties of LWFA-generated electron beams [2, 3]. Experiments have used gas jet targets to provide distinct regions for the different accelerating schemes, separated by thin foil plasma mirrors which terminate the laser-driven acceleration. The PWFA-driven section was sometimes ionised before the arrival of the electron beam using a counter-propagating low-

intensity laser pulse, and either mechanically or laser-induced shocks in the gas flow were used to localise injection of a witness buch to minimise energy spread. These experiments have observed 100 MeV energy gain of the witness bunch, and some mitigation of stability issues inherent to LWFA generated beams.

Here we report measurements of GeV level energy gain of an LWFA-generated electron beam when using a dual-stage gas cell target. A low divergence 1 GeV energy electron beam was generated and propagated through a thin-film plasma mirror into a second, lower-density plasma acceleration stage. When preionised using a secondary laser pulse, energy gain was sometimes were observed for parts of the spectrum. The peak energy reached was $(4.0^{+0.4}_{-0.3})$ GeV. The mechanism behind this acceleration and the implications of these measurements are discussed.

2 Experimental Setup

This experiment used both beams of the Gemini laser system. The South beam was focused using an $f = 6$ m off-axis parabola to an elliptical spot with mean FWHM radii of $((24 \pm 2)\,\mu\text{m}, (22 \pm 1)\,\mu\text{m})$. An $f = 7.5$ m spherical dielectric mirror was used to focus the North beam to a spot size of $((24 \pm 4)\,\mu\text{m}, (19 \pm 1)\,\mu\text{m})$. The post-compression energy in the South and North beams was (11.2 ± 0.3) J and (8.9 ± 0.4) J respectively and was kept constant for all laser shots reported here.

The target consisted of two independent gas cells, as shown schematically in Fig. 1. The first gas cell operated with a length of 6.9 mm, and was filled with helium gas with a 2% nitrogen dopant by weight. For the data reported here, the plasma density in cell 1 was $(2.5 \pm 0.3) \times 10^{24}\,\text{m}^{-3}$. A shaped aperture at the exit of the cell produced an extended density down-ramp that aided in the collimation of the electron beam, reducing the divergence to the sub-milliradian level [4]. A 125 µm thick Kapton tape positioned 5 mm after the exit of the first gas cell could be used as a thin-film plasma mirror to simultaneously dump the South laser and redirect the North laser pulse onto the optical axis. The position of the North beam focus was 9 mm after the tape, which was found to maximise the intensity at focus. The second cell was placed with its entrance aperture 5 mm after the tape. The length of this cell was 20 mm and the density was $(1.3 \pm 0.2) \times 10^{24}\,\text{m}^{-3}$.

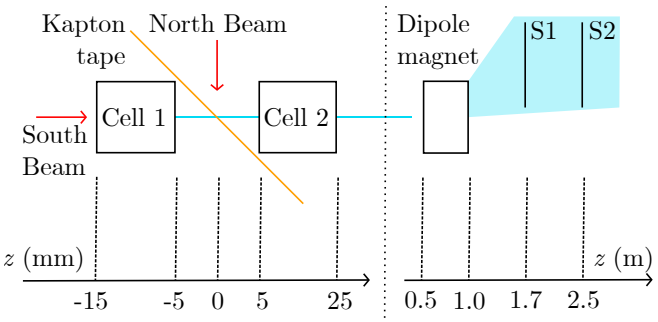

Figure 1: Simplified diagram of the experiment setup. S1 and S2 indicate the position of screen 1 and screen 2.

Fine synchronisation of the laser pulses was achieved by maximising the contrast of the interference pattern formed when spatially overlapping the laser pulses; an interference pattern was only observed when the delay was within 100 fs. Long-timescale synchronisation drift was monitored using spectral interferometry of leakage light, and was periodically corrected. Spatial overlap of the laser pulses was achieved by simultaneously imaging both focal spots with the same microscope after the tape, and then the pointing was monitored using leakage light from one of the turning mirrors after the focusing optics.

A 1 T 0.5 m long permanent dipole magnet dispersed the electrons vertically onto two Scintacor Luminex regular scintillating screens, which were imaged onto 16-bit sCMOS sensors. The first screen detected electrons with $0.1\,\text{GeV} \lesssim E \lesssim 2\,\text{GeV}$, while the second screen measured the $0.8\,\text{GeV} \lesssim E \lesssim 4\,\text{GeV}$ energy range, with the exact bounds sensitive to the assumed angle between the electron beam and the horizontal plane. As shown in Fig.1, the medium energy and high energy screens were at

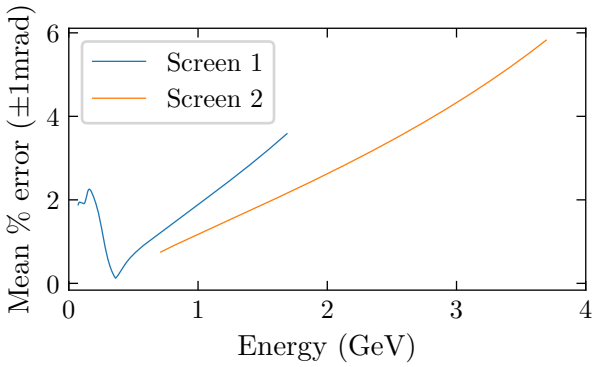

Figure 2: The mean % energy error that results from pointing fluctuations into the electron spectrometer of ±1 mrad along the dispersion plane, averaging over the positive and negative directions.

$z = 1.7\,\mathrm{m}$ and $2.5\,\mathrm{m}$ respectively. Mirrors were used to offer a line of sight from the cameras to the screens, and were angled such that the image plane of the camera lenses was parallel to the screens, maximising resolution across the scintillators. Minor viewing angle distortions were corrected by using affine transformations. Strong vignetting of screen 1 was mitigated by imaging a green light source placed at different places along the screen. The absolute charge was calibrated using Fujifilm BAS-TR image plate.

A particle tracking code calibrated screen position to electron energy. Pointing angle variation along the dispersion plane obfuscates energy measurements, and this effect is more significant at higher energies due to the increased beam rigidity. This is quantified in Fig. 2, where the error on the energy over an input angle variation of ±15 mrad is plotted against energy. The spectral overlap between the two screens can be used to mitigate the uncertainty resulting from pointing jitter [5]. This is the region from 0.8 GeV to 1.7 GeV in Fig. 2. By identifying common features in the spectrum on each screen in this region, the assumed input angle can be modified until the two measurements agree, thereby reducing the effects of pointing error for this part of the spectrum.

3 Experimental Results

Fig. 3 shows example electron spectrometer images, all taken with both laser pulses in use. Panels 3(a-c) show unperturbed electron spectra, representative of spectra observed when the North beam was inactive or when there was no gas in cell 2. The mean charge of the beam for energies above 150 MeV was $(140 \pm 40)\,\mathrm{pC}$, where the range indicates the shot-to-shot standard deviation. Panels 3(d-g) correspond to shots where the electron beam has been modulated by the plasma in the second cell, resulting in energy gain. The energy gain is accompanied by the breaking of the beam into multiple beamlets, a decrease in the energy of parts of the beam, and enhanced oscillations in the beam pointing as a function of energy. Strong modulations were only observed on approximately 10% of shots, with only a subset of these resulting in an above-baseline peak energy gain.

To make an accurate high energy spectrum measurement, the electron beam pointing angle into the magnet must be determined. This will be done using both statistical measurements of the beam pointing, and the feature matching procedure described in the previous section. Fig. 4 shows the average electron beam pointing angle of 125 shots relative to the optical axis shots, calculated using the beam's centre of mass on the electron profile diagnostic. The average pointing was $[\theta_x, \theta_y] = [(8\pm1)\,\mathrm{mrad}, (6\pm3)\,\mathrm{mrad}]$, where the range indicates the standard deviation. Since the electron spectrometer dipole magnet deflects the beam in the positive y direction, the beam profile data indicates that assuming a flat input angle will underestimate the energy.

The large pointing variation necessitates shot-wise pointing measurements. Fig. 5 shows the feature matching performed to estimate the input angle for the energy measurement, using the data in Fig. 3(f). The disagreement between the absolute values of dQ/dE arises from the vignetting correction that was only performed for screen 1. As θ_y changes, the spectra extracted from each screen are altered in slightly differ-

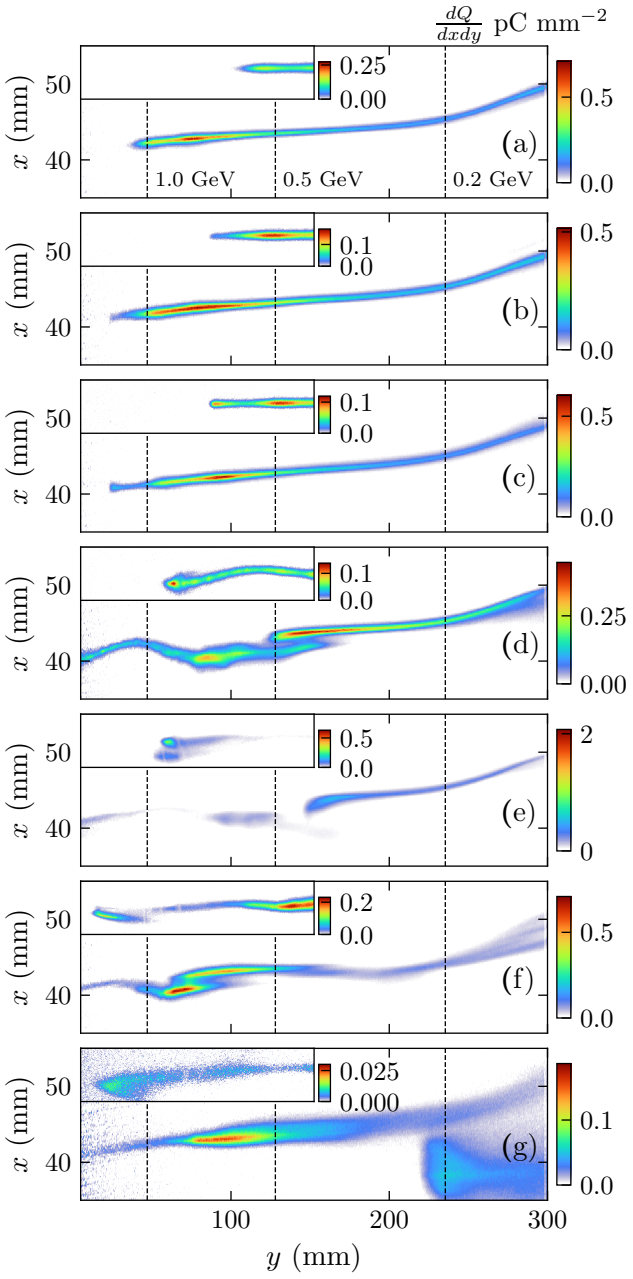

Figure 3: Example images from the electron spectrometer screens. The large figure is from screen 1 and the inset is from screen 2. The inset colourbars have units $dQ/(dxdy)$ in pC mm^{-2}. Panels (a-c) show unperturbed beams, similar to those seen without the North beam. Subplots (d-g) show beams after propagating through the plasma in the second cell, resulting in an energy boost for some electrons and transverse modulations of the beam.

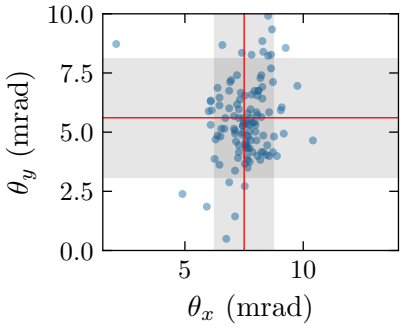

Figure 4: Pointing of electron beam on measured by the beam profile monitor.

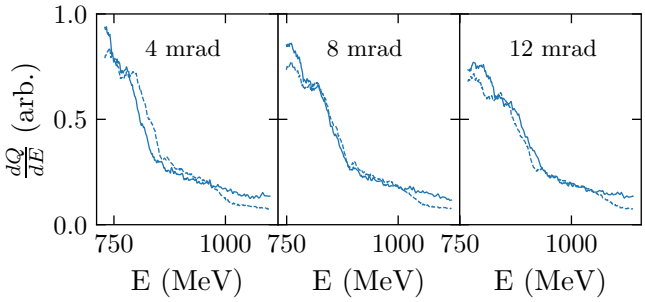

Figure 5: The electron beam spectra from the shot in Fig. 3(f) overlap region, plotted for different values of θ_y. The solid and dashed lines are the spectra from screens 1 and 2 respectively.

ent ways due to the different screen locations. The best fit is obtained by empirically matching peaks in the spectra, which for this shot gives $\theta_y = (8 \pm 1)$ mrad, where the uncertainty indicates the range of plausable angles. While theoretically this procedure can be performed for any spectrometer measurements where there is an overlap between the two screens, in practice, it is most reliable when there are features in the beam.

Fig. 6 shows the image from the high energy screen in Fig. 3(f), with selected energy contours. Oscillations in the x direction have an amplitude not larger than 10 mm, which equates to $\Delta\theta_x = 2$ mrad. Using this value to estimate the uncertainty, the peak energy of this electron beam is $(4.0^{+0.4}_{-0.3})$ GeV, where the asymmetric error comes from pointing causing an increasing fraction of the error at higher energies.

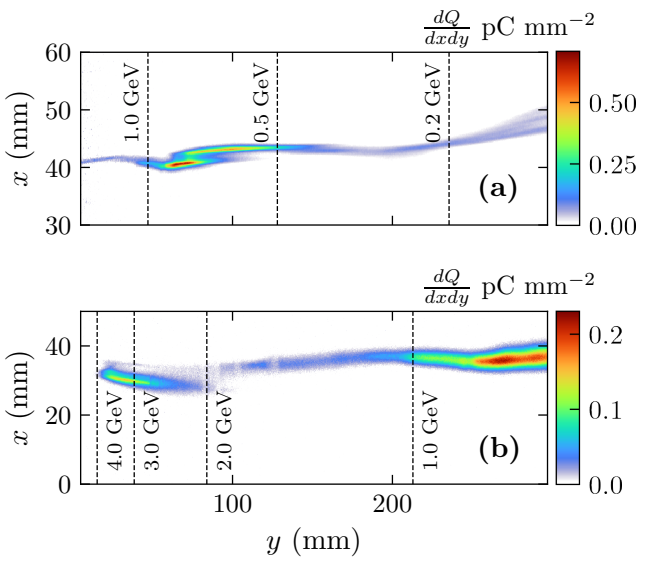

Figure 6: Images from the electron spectrometer overlaid lines indicating the energy reached using the estimated input angle of $\theta = 8\,\text{mrad}$.

4 Discussion

We believe that the primary driver of the energy gain is the electron beam itself, rather than the second laser pulse. This is because measurements of the reflected pulse intensity indicate that the laser would be too weak to drive a plasma wave capable of causing the observed energy gains. Further, parts of the electron beam appeared to be decelerated on shots with large transverse modulations, indicating absorption of electron beam energy by the plasma. On the other hand, it is surprising that the beam was affected on only a fraction of the shots despite always propagating through plasma in the second cell. This inconsistency could indicate that the reflected laser may be having some effect.

We can use the measured beam parameters to estimate the electron bunch density, n_b, when it enters the second cell. For an electron beam with a charge of 140 pC, 0.2 mrad divergence, a source size of 1 µm, and a bunch length of ck_p, where k_p is the plasma wavenumber in cell 1, $n_b = 1 \times 10^{25}\,\text{m}^{-3}$ when it enters cell 2. This would drive a large-amplitude plasma wave in the second cell, where the plasma density $(1.3\pm0.2)\times10^{24}\,\text{m}^{-3} \ll n_b$, which would be capable of trapping and accelerating electrons. The injection dynamics and the maximum achievable energy depend acutely on the current profile, which was not measured during the experiment. Given the varied current profiles that LWFA can produce, it is possible that a profile capable of achieving such high energy gains could have been generated in the first cell [6]. Particle-in-cell simulations will be run to investigate this process.

The large energy gains measured here exceed those observed in similar experiments where gas jets were used. These results indicate that there may be benefits to using gas cells for PWFA stages, as envisioned in [1]. Gas cells permit a degree of control over the density profiles at the plasma entrance and exit, and provide a more homogeneous plateau region [7], making the strongest accelerating fields at the rear of the wave more accessible for witness electrons [8]. If the injection of electrons into the wake can be made more reliable, then a scheme such as the one presented here could be a useful method for compactly boosting the peak energy of LWFA-generated electron beams.

The authors acknowledge funding from STFC (ST/J002062/1, ST/P002021/1, ST/V001639/1), and technical support from the CLF.

References

[1] A. Martinez de la Ossa et al., *Phil. Trans. R. Soc.*, **377**, 20180175 (2019).
[2] J. P. Couperus Cabadağ al., *Physical Review Research*, **3**, L042005 (2021)
[3] F. M. Foerster et al., *Physical Review Special Topics - Accelerators and Beams*, **12**, 041016 (2022)
[4] M. P. Backhouse et al., *CLF annual reports*, "Low divergence electron beams from a gas cell", (2024)
[5] H. J. Cha et al., *Review Scientific Instruments*, **83**, 063301 (2012)
[6] G. Loisch et al., *Physical Review Letters*, **121**, 064801 (2018)
[7] S. Kuschel et al., *Physical Review Letters*, **121**, 154801 (2018)
[8] K. Poder et al., *Physical Review Letters*, **132**, 195001 (2024)